Shielding Effects in Microstrip Discontinuities

LAWRENCE P. DUNLEAVY AND PISTI B. KATEHI, MEMBER, IEEE

Abstract—**As an application of the theoretical method described in a companion paper (pp. 1758–1766, this issue), numerical and measured results are presented for open-end and series gap discontinuities and a coupled line filter. Comparisons are also made to commercially available CAD package predictions. The results verify the accuracy of the new theoretical method and demonstrate the effects of shielding on discontinuity behavior. The experimental techniques used, which involve the through-short-delay de-embedding approach, are also explained.**

I. INTRODUCTION

THIS IS THE second of two papers concerned with the study of shielding effects in microstrip discontinuities. The companion paper [1] develops a new theoretical method for the full-wave analysis of shielded microstrip discontinuities. The effects of shielding are important in two situations. The first is when the frequency approaches or is above the cutoff frequency for higher order mode propagation. The second occurs when the metal enclosure (Fig. 1) is physically close to the circuitry (proximity effects). These effects have not been adequately studied in the past, and are not accounted for in the discontinuity models in most available CAD packages.

In addition to improved theoretical methods, there is a great need for experimental data. Published experimental data on microstrip discontinuities are very limited, especially for high microwave (above *X*-band) and millimeter-wave frequencies. Such measurements are not trivial, but are essential for verification of the theoretical method. This need motivated the experimental study discussed here.

This paper uses the previously described method [1] to study the effects of the shielding cavity on the behavior of one- and two-port discontinuities including open ends, series gaps, and parallel coupled line filters. Comparisons are made to measurements, to available data from other full-wave analyses, and to commercially available CAD packages.

II. EXPERIMENTAL TECHNIQUES

Measured data on microstrip discontinuities are very limited, particularly at higher frequencies (above 10 GHz). This is due to the difficulties encountered in performing accurate microstrip measurements. In order to measure a microstrip circuit, it is generally mounted in a test fixture with either coax-to-microstrip or waveguide-to-microstrip transitions. The main difficulties associated with such measurements are the separation of test fixture parasitics from measurements, called de-embedding, and the nonrepeatability of microstrip connections.

This section explains the experimental techniques used for this study and addresses the connection repeatability issues that pertain to the measurements.

A. De-embedding Approach

The measurement approach of this study employs automatic network analyzer (ANA) techniques in conjunction with the through-short-delay (TSD) method for de-embedding the effects of the test fixture from the measurements. The test fixture that was used is shown in Fig. 2. The fixture employs a pair of 7 mm "Eisenhart" coax-to-microstrip transitions [2]. The shielding is provided by placing U-shaped covers on top of the microstrip carriers. This forms a cavity similar to that of Fig. 1. The instrument used for the measurements was an HP8510 ANA.

The test fixture invariably introduces unwanted parasitics and a reference plane shift to the measurements. These effects must be accurately accounted for and removed from the measurements, or incorporated into the ANA system error model. Conventional ANA calibration, which uses a short circuit, an open circuit, and a matched load, is not easily performed in microstrip since these calibration standards are much more difficult to realize in microstrip.

The process for removing test fixture effects is called de-embedding and consists of two steps: 1) fixture characterization and 2) the extraction of fixture parasitics. Through de-embedding, the effective calibration reference planes are moved from the coaxial or waveguide ANA test ports to microstrip test ports within the fixture.

A comparison of various de-embedding techniques [3] lead to the choice of the TSD technique for the experimental study. This approach was selected over the alternatives considered because the standards used for fixture characterization are the easiest to realize in microstrip and because the connections to these standards can be made in the same way as the connections made to discontinuity test circuits. In the TSD technique, two-port measurements made on a through (zero length delay) line, a "short" circuit, and a delay line provide enough information to characterize the fixture. Since the original paper [4], it has

Manuscript received April 19, 1988; revised August 19, 1988. This work was supported primarily by the National Science Foundation under Contract ECS-8602530. Support was also provided by the Army Research Office under Contract DAAL03-87-K-0088 and by the Microwave Products Division of the Hughes Aircraft Company.

L. P. Dunleavy was with the Department of Electrical Engineering and Computer Science, University of Michigan, Ann Arbor. He is now with the Industrial Electronics Group, Hughes Aircraft Company, Torrance, CA.

P. B. Katehi is with the Department of Electrical Engineering and Computer Science, University of Michigan, Ann Arbor, MI 48109-2122.

IEEE Log Number 8824530.

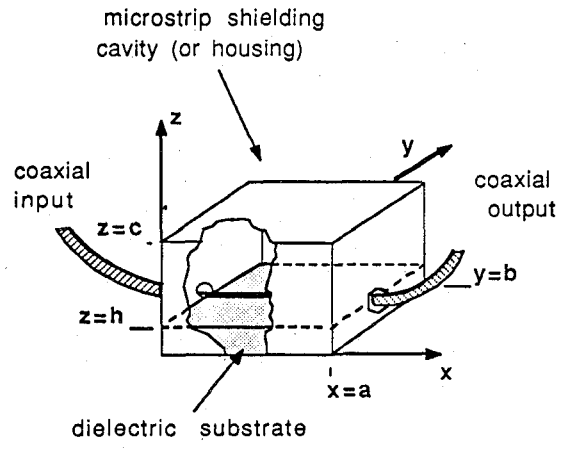

Fig. 1. Basic geometry for the shielded microstrip cavity problem.

been pointed out that the "short" implied in TSD need not be perfect. In fact, any highly reflecting standard may be used in its place [5], [6]. The only requirement is that the same reflection coefficient Γ_s must be presented to both microstrip test ports.

This measurement approach provides for the measurement of the effective dielectric constant, the reflection coefficient of open-end discontinuities, and the two-port scattering parameters of series gaps and coupled line filters. In the present implementation of TSD de-embedding, an open-ended microstrip line is used in place of the short as the reflection standard. Measurements of microstrip effective dielectric constant ϵ_{eff} and of the reflection coefficient of the open-end Γ_{op} are obtained as by-products of the fixture characterization procedure. Once the fixture is characterized, the de-embedded S-parameter measurements of two-port discontinuities are obtained by extracting the fixture parasitics mathematically.

B. Connection Repeatability Issues

One drawback to the TSD technique is that good microstrip connection repeatability is important for accuracy. Microstrip connections are much harder to make and are less repeatable than connections in coax and waveguide. This is a key limiting factor to the accuracy of microstrip measurements at higher frequencies. To address this issue, a microstrip connection repeatability study was carried out [7]. The results of this study were used to decide on the best connection approach to use and to estimate the associated measurement uncertainties.

There are three basic connection alternatives for TSD characterization of a coaxial fixture. Each of these must rely on at least one of the following assumptions:

1) repeatability of connections made from the coax-to-microstrip transition to the microstrip line;
2) repeatability of microstrip-to-microstrip interconnects;
3) uniformity of electrical characteristics between different transitions (launcher-to-launcher uniformity).

The results of the repeatability study favor a connection approach relying on repeatable coax-to-microstrip connections, and this was the approach adopted for the present work.

As part of this work, a method was developed to approximate the uncertainties in de-embedded results arising from connection repeatability errors [3]. The analysis consists of perturbing the S parameters of the TSD standards and the DUT with a set of experimentally derived error vectors that are representative of the variations of each S-parameter (S_{11}, S_{12}, etc.) measurement with repeated connections. Software was written to allow processing of the perturbed S-parameter data in the same way that the measurement data are processed during the TSD de-embedding procedure discussed above. This perturbation analysis shows approximately how connection errors—which are inevitable—propagate through the TSD mathematics and limit the precision of the final results.

III. Numerical and Experimental Results

In this section, the numerical and experimental results of the present research are presented for the network parameters of shielded microstrip discontinuities. Included here are results for the effective dielectric constant, open-end and series gap discontinuities, and coupled line filters. Where possible, comparisons are made to results generated from the commercially available CAD packages Super Compact and Touchstone.[1]

The CAD models used in these packages are based on a combination of different theoretical techniques, most often embodied in simplified closed-form solutions, curve fit expressions, or look-up tables. These models do not adequately account for the effects of the shielding box (Fig. 1). Further, in simulating a circuit containing many discontinuities, the analysis of these packages assume that the discontinuities are independent of one another and the matrix representations for each discontinuity are simply cascaded together mathematically.

In contrast, the full-wave solution presented in the companion paper [1] accurately treats the entire geometry of the shielded microstrip circuit as a boundary value problem. The interactions between the discontinuity structure, adjacent microstrip conductors, and the shielding cavity are automatically included in the analysis. Because of this, the method is expected to provide better accuracy than CAD model predictions.

A. Cutoff Frequency and Higher Order Modes

One case where shielding effects are noticeable is when the frequency approaches the cutoff frequency f_c for the first higher order shielded microstrip mode. The nature of higher order modes in shielded microstrip is quite different from that in open microstrip. In open microstrip, higher order modes occur in the form of surface waves and radiation modes. The first surface wave mode has a cutoff frequency of zero. In shielded microstrip, the higher order

[1]Super Compact and Touchstone are microwave CAD software packages available from Compact Software and EESOF, respectively.

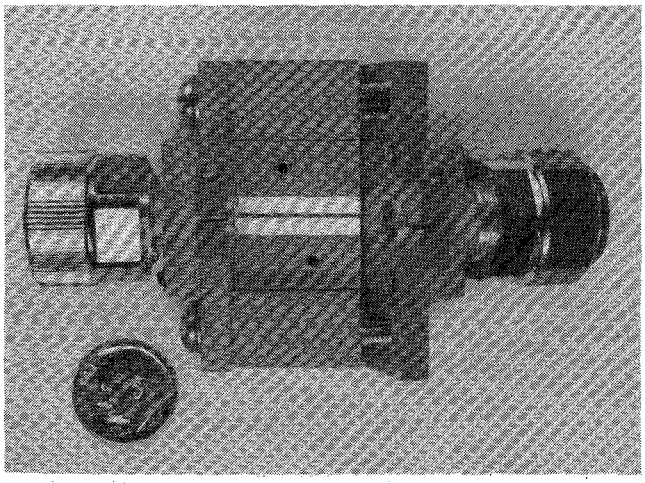

Fig. 2. 7 mm coaxial/microstrip test fixture (partially disassembled) used for measurements.

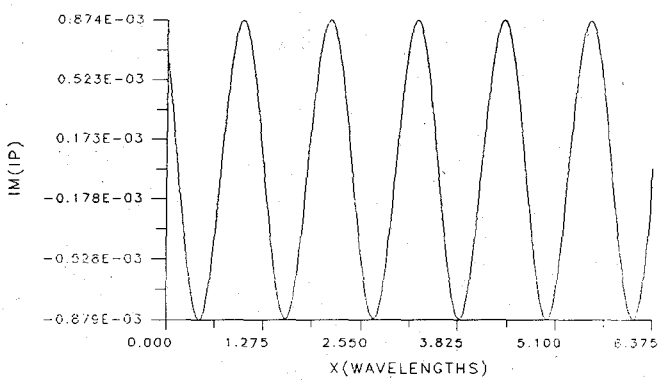

Fig. 3. Imaginary part of current on open-ended line below the cutoff frequency f_c ($f = 16$ GHz, $\epsilon_r = 9.7$, $W/h = 1.57$, $h = .025$ in, $b = c = 0.275$ in).

modes take the form of waveguide modes [8]. As a consequence, below the waveguide cutoff frequency, only the dominant microstrip mode can exist.

For the present work, the f_c for the shielded microstrip geometry of Fig. 1 is approximated by considering the dielectric-loaded waveguide formed by removing the strip conductors and the walls at $x = 0$ and a. The cutoff frequencies thus derived have been found to give a good prediction of where higher order effects are first observed in the computed current distributions. As an example, Fig. 3 shows the current distribution on an open-ended line operating below the cutoff frequency. For the indicated geometry, f_c is about 17.9 GHz. As the frequency is raised above the cutoff frequency, the current becomes more and more distorted, as shown in Fig. 4. The distortion is due to the interactions between the dominant mode and the first higher order waveguidelike mode inside the cavity.

B. Effective Dielectric Constant

Fig. 5 shows ϵ_{eff} for a 25-mil-thick alumina substrate where the cross-sectional shielding dimensions, b and c, are ten times the substrate thickness h. The numerical results are compared to measurements and to CAD package predictions. Note that Super Compact allows only the cover height to be varied while the calculation provided by Touchstone neglects shielding effects. For the shielding geometry used here, it is seen that the difference between the numerical and the CAD package results is within experimental error. However, interestingly enough, better agreement between the CAD results and the numerical results is observed at higher frequencies. This may be due to the fact that the sidewalls, which are not included in the CAD package analysis, are electrically closer to the strip at low frequencies.

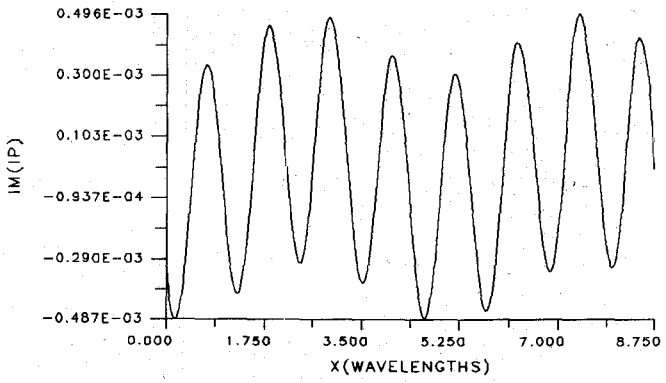

Fig. 4. Open-ended microstrip current above f_c ($f = 22$ GHz, $\epsilon_r = 9.7$, $W/h = 1.57$, $h = .025$ in, $b = c = 0.275$ in).

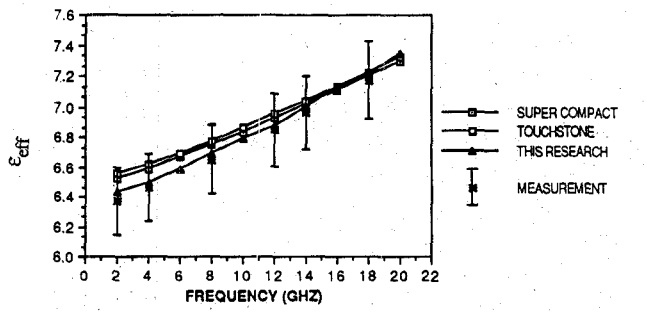

Fig. 5. Numerical results for ϵ_{eff} compared with measurements and CAD package predictions ($\epsilon_r = 9.7$, $h = .025$ in, $b = c = 0.25$ in).

The measured data are obtained as a by-product of the TSD fixture characterization procedure, as discussed above. The data shown represent the average of ten separate procedures conducted over a period of time with four different sets of TSD standards. The error bars shown in Fig. 5 represent the standard deviation ($\pm s$) of the different measurements. This data are shown here in lieu of the result from a single measurement, since they give a more representative view of the involved measurement uncertainty. In this case the error bars shown represent the combined effect of connection errors, variations in ϵ_r, and other factors. The major error source in this case is believed to be the variations in ϵ_r, which can be significant for alumina substrates [9].[2]

To see how ϵ_{eff} varies with shielding, consider the plot of Fig. 6. This plot compares numerical and Super Com-

[2]This error reflects the uncertainty in knowing which value of ϵ_r to use in the theoretical simulations.

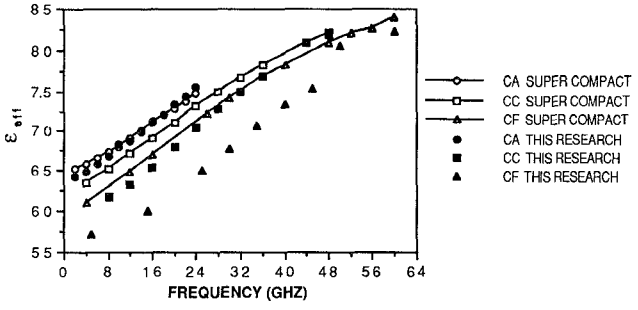

Fig. 6. Shielding effects on ϵ_{eff} for an alumina substrate (see Table I for geometry).

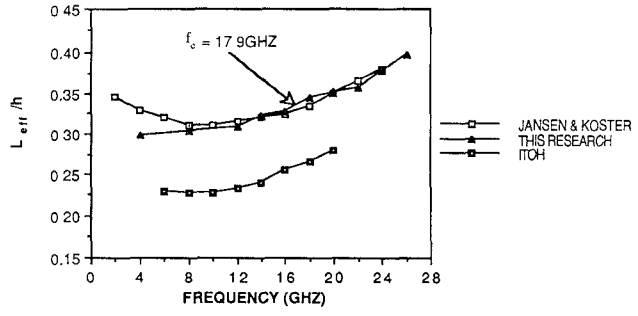

Fig. 8. Numerical results compared to those from other full-wave analyses ($\epsilon_r = 9.6$, $W/h = 1.57$, $b = 0.305$ in, $c = 0.2$ in, $h = 0.025$ in)

TABLE I
CAVITY NOTATION USED TO DENOTE DIFFERENT GEOMETRY AND SUBSTRATE PARAMETERS

CAVITY	ϵ_r	W (in)	h (in)	b (in)	c (in)	f_c (GHz)
CA	9.7	.025	.025	.250	.250	21.8
CC	9.7	.025	.025	.100	.100	37.5
CF	9.7	.025	.025	.075	.075	41.7
QCB	3.82	.0157	.010	.122	.080	45.8
QCE	3.82	.0157	.010	.100	.100	73.0
QCG	3.82	.0157	.010	.050	.05	102.5

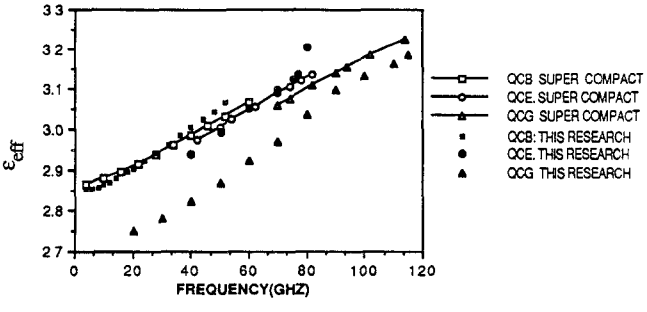

Fig. 7. Shielding effects on ϵ_{eff} for a quartz substrate (see Table I for geometry).

TABLE II
COMPARISON OF L_{eff}/h COMPUTATION FOR THE TWO TYPES OF EXCITATION METHODS

f (GHz)	4	8	12	14	16	18	20
GAP GENERATOR	.298	.305	.309	.321	.324	.344	.353
COAXIAL EXCITATION	.299	.304	.309	.322	.327	.344	.352

pact results for three different shielding geometries. The notation used to describe different shielding and substrate geometries is explained in Table I.

In all cases, as the shielding is brought closer to the microstrip, a reduction in ϵ_{eff} is predicted. The case for cavity CA is the same as that in Fig. 5. For the other two cases, where the shielding is closer to the microstrip, the Super Compact shows a smaller effect than the present integral equation method predicts.

The effect of shielding on ϵ_{eff} for a quartz substrate is displayed in Fig. 7. In this case the Super Compact analysis is seen to give good results for both of the two larger shielding geometries. However, the numerical results again show a larger reduction in ϵ_{eff} as the size of the shielding is decreased further.

The reduction of the effective dielectric constant, relative to Super Compact, can be explained as follows. For a larger shielding geometry, the field distribution on the microstrip more closely resembles the open microstrip case, with most of the electric field concentrated in the substrate. In this case, most of the electric field lines originate on the microstrip conductors and terminate on the ground plane below. As the cavity size is reduced, the ground planes of the top walls and sidewalls are brought closer to the microstrip lines. The electric field distribution is now less concentrated in the substrate, as more field lines can terminate on the top walls and sidewalls. As a result, a proportionally larger percentage of the energy propagating down the line does so in the air region, and the dielectric constant is reduced.

C. Open-End Discontinuity

As discussed in [1], an open-end discontinuity can be represented by an effective length extension L_{eff} or by a shunt capacitance c_{op}. Both of these representations will be used in this section.

The plot of Fig. 8 compares L_{eff} results to those of Jansen *et al.* [10] and Itoh [11]. In this case, the dimensions of the shielding cavity are large with respect to the substrate thickness. The results from this research are almost identical to those obtained by Jansen *et al.* for frequencies above 8 GHz but show a reduced value for lower frequencies.

The case of Fig. 8 was chosen to compare the coaxial and gap generators excitation methods used in the method of moments solution. Table II shows that the results computed for this case by the two methods are equivalent. This equivalence also holds for the two-port scattering parameters for the structures considered herein. Hence, as far as computing network parameters is concerned, either method gives good results. Since the coaxial method is more realistically based, this conclusion lends validity to the use of the gap generator method.

The results shown in Fig. 9 illustrate the effect of shielding on the open-end discontinuity. The normalized open-end capacitance c_{op} is plotted for three different

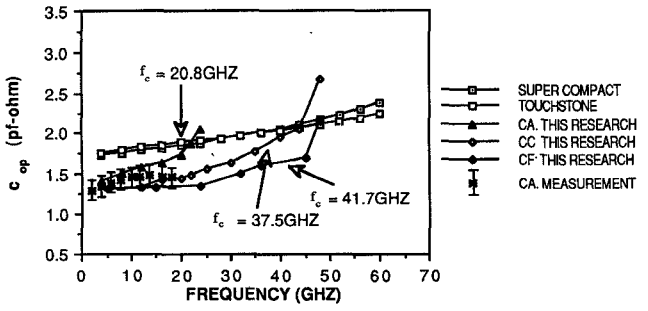

Fig. 9. Comparison of the normalized open-end capacitance for three different cavity sizes. This shows that shielding effects are dominated by the onset of higher order modes rather than by proximity effects (see Table I for cavity geometries).

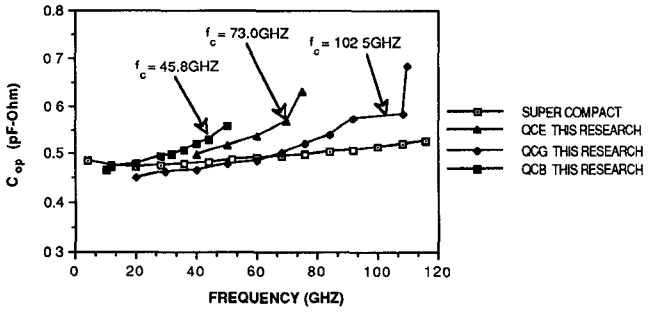

Fig. 10. Normalized open-end capacitance for three different cavity sizes for a quartz substrate. These results also show the strong dependence of the capacitance on f_c (see Table I for cavity geometries).

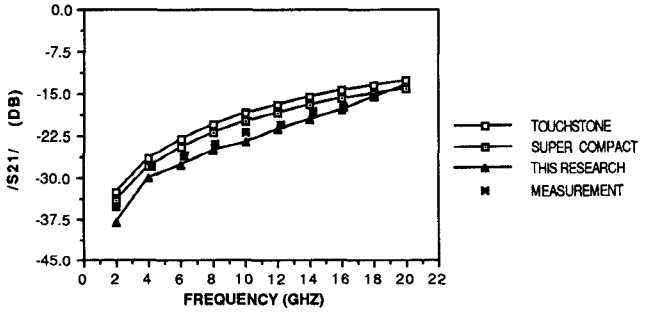

Fig. 11. Results for the magnitude of S_{21} for a 15 mil series gap.

cavity sizes. The results show that reducing the cavity size raises f_c (as expected) and lowers the value of c_{op}. For comparison, data obtained from Super Compact and Touchstone and measurements are included. The errors bars on the measurements represent the estimated standard deviation ($\pm s$) of the connection errors associated with this measurement.[3]

Similar shielding effects are observed for an open end on a quartz substrate, as shown in Fig. 10. In this case it is seen that the Super Compact result gives a good value for low frequencies, and where the frequency is well below the cutoff frequency for a given shielding size. These results show that shielding effects due to wall proximity are less

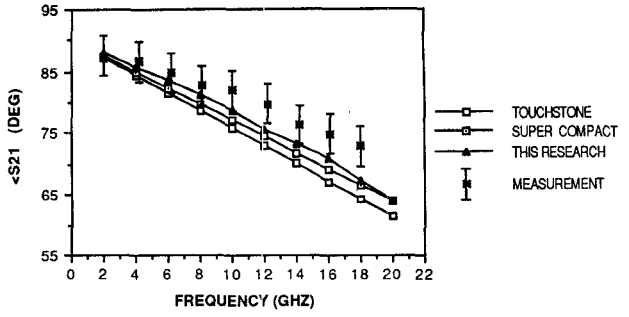

Fig. 12. Results for the angle of S_{21} for a 15 mil series gap.

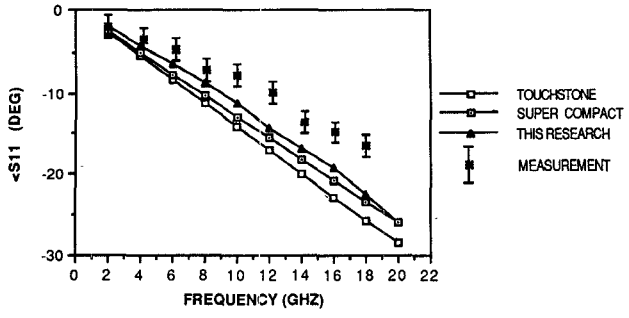

Fig. 13. Results for the angle of S_{11} for a 15 mil series gap.

important than shielding effects due to the onset of higher order modes.

D. Series Gap Discontinuities

Numerical and experimental results have been obtained for series gap discontinuities of three different gap widths [3]. Results for one of these gaps are presented here.

Numerical results for the magnitude of S_{21} of a series gap with a 15 mil gap width are shown plotted in Fig. 11. For comparison, results obtained using Super Compact and Touchstone are also shown plotted along with measured data. The numerical results are seen to be in very good agreement with the measurements. The test substrate and shielding dimensions used for the measurements are those for cavity CA (Table I). The error bars associated with the connection errors are on the order of ± 0.5 dB and are too small to show on the plots.

Results for the angle of S_{21} and S_{11} for the 15 mil series gap are shown in Figs. 12 and 13. The error bars in these charts represent the estimated standard deviation from the perturbation analysis.[4] Although the measurements tend to favor the numerical results, the phase differences are not too significant since it is suspected that the measurement may be in error by more than that attributed to connection errors alone. The phases of the S parameters for the two other gaps behave in a way similar to that for the 15 mil gap and have been omitted from this treatment.

These results are seen to further verify the theory developed in the companion paper [1]. For the large shielding

[3]The other error sources indicated for the effective dielectric constant measurement are not considered to be as significant for this measurement.

[4]The analysis was carried out at 10 GHz, and it is assumed that the connection errors are approximately the same at the other measurement frequencies.

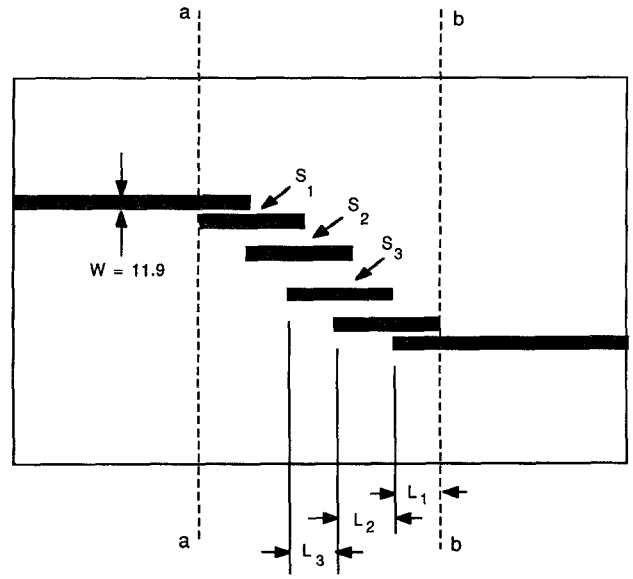

Fig. 14. Sketch of four-resonator coupled line filter studied here ($\epsilon_r = 9.7$, $h = 0.025$ in, $b = 0.4$ in, $c = 0.25$ in).

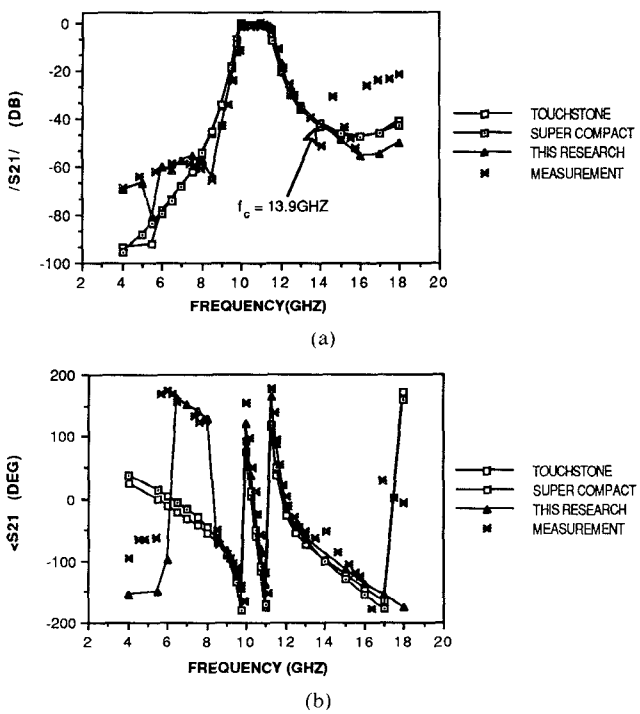

Fig. 15. Results for transmission coefficient S_{21} of four-resonator filter ($\epsilon_r = 9.7$, $W = 0.012$ in, $h = 0.025$ in, $b = 0.4$ in, $c = 0.25$ in).

dimensions used for the measurements ($b, c \gg h$) the CAD models are also seen to give reasonable predictions. The behavior of series gaps for different shielding dimensions was not studied; instead emphasis was placed on obtaining results for coupled line filters since their behavior is more complicated and therefore more interesting.

E. Four-Resonator Coupled Line Filter

The last results to be presented are for the four-resonator coupled line filter of Fig. 14. For brevity, only the amplitude and phase of S_{21} will be discussed.

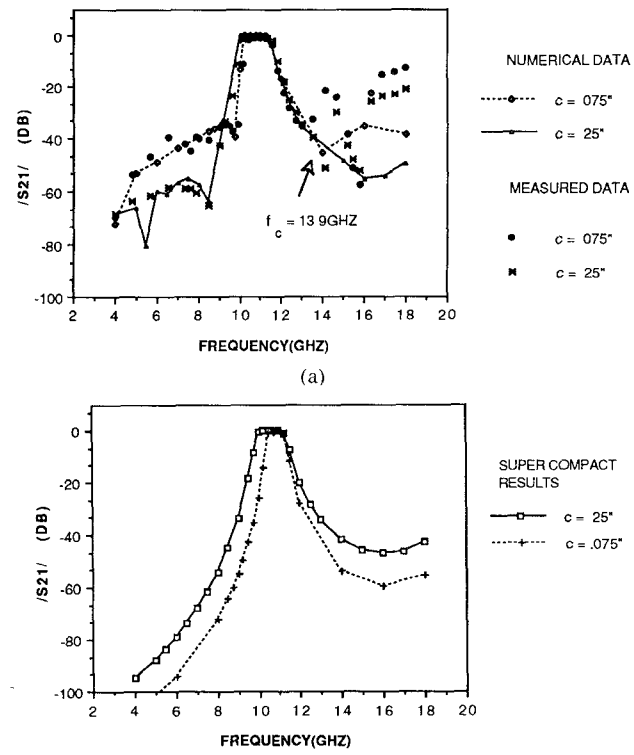

Fig. 16. Results for lowering the shielding cover on the amplitude response of four-resonator filter ($\epsilon_r = 9.7$, $W = 0.012$ in, $h = 0.025$ in, $b = 0.4$ in).

Numerical and measured results of this research are compared along with CAD model predictions in Fig. 15. The CAD package analysis for coupled line filters is performed by cascading two different types of discontinuity elements together: coupled microstrip lines and open-end discontinuities. Neither of the packages studied here accounts for shielding in the open-end discontinuity model; however, Super Compact does include the effect of the cover height in the model for coupled lines.

The numerical results shown in Fig. 15 demonstrate excellent agreement with measurements up to the cutoff frequency. The cutoff frequency f_c for the shielding geometry of the filter is approximately 13.9 GHz. Above this frequency, the measurements are distorted because of the enhanced electromagnetic coupling between the feed apertures. This coupling is due to the excited waveguide modes within the test fixture.

The results of Fig. 15 show that even for large shielding dimensions discrepancies are apparent in the CAD model predictions, whereas the numerical results follow the measurements closely, both in amplitude and phase. As can be seen from the amplitude response (Fig. 15(a)), the CAD models give a good prediction in the passband, but fail to predict the filter response in the rejection band. This is also seen from the phase response (Fig. 15(b)), where the CAD models display a large error compared to measurements between about 6 and 8.5 GHz, while the numerical results track the measured amplitude and phase very well.

Below about 5.5 GHz the measured phase is seen to be different from the predictions of both the CAD models

and the numerical results. This is probably due to a phase error in the measurements. In the TSD technique, the delay line for the measurements should ideally be $\lambda_g/4$ at the measurement frequency.[5] When the electrical length becomes either too short or too close to a multiple of $\lambda_g/2$, phase ambiguities can result. A good rule of thumb is for the delay line to be between $\lambda_g/8$ and $3\lambda_g/8$. At 5.5 GHz the delay line used for the measurements is slightly less than $\lambda_g/8$; hence, this is most likely the source of the phase error in the measurements below this frequency.

We will now examine what happens as the top cover is brought closer to the circuitry. Fig. 16(a) shows Super Compact predictions for the four-resonator filter with two different cover heights. These predictions indicate that lowering the cover height should significantly narrow the passband and reduce the amplitude in the rejection band.

A significantly different prediction is observed in the numerical results for the case presented in Fig. 16(b). A narrowing of the passband response is also observed in the numerical predictions, but not by nearly as much as Super Compact predicts. More importantly, the amplitude in the rejection band is seen to increase instead of decrease.

To prove that the numerical prediction is indeed the correct one, an additional measurement was made of the filter for the low cover height case. As can be seen from Fig. 16(b) the agreement between measured data and the numerical predictions from this research is excellent.

IV. Summary

In this paper theoretical and experimental results were presented for the network parameters of one- and two-port discontinuities. For the measurements, the TSD de-embedding approach was used. Connection repeatability errors were considered in detail and a perturbation analysis was developed to approximate their effect on the precision of the final de-embedded results.

The effects of shielding on microstrip behavior were studied. It was demonstrated that the computed current distribution becomes distorted above the cutoff frequency f_c for the first higher order shielded microstrip mode. On the other hand, as long as the cavity size is such that the frequency is below f_c, the current is uniform and undistorted regardless of how thick the substrate is.

Only one of the CAD packages studied takes shielding into account for the effective dielectric constant (ϵ_{eff}) calculation, and then only cover effects are considered. A comparison of the CAD package predictions with the numerical results of this research for ϵ_{eff} showed that good agreement is obtained when the shielding dimensions are large with respect to the substrate thickness, while for small shielding dimensions, the difference between the different results becomes significant.

For the open-end discontinuity, good agreement with other full-wave solutions and with measurements has been demonstrated. A comparison of open-end capacitance for different cavity sizes showed that, as the cutoff frequency is approached, the capacitance increases in each case. Choosing a small cavity with a high cutoff frequency extends the region where the capacitance is relatively constant.

Good agreement between numerical and measured results was also demonstrated for series gap discontinuities and a four-resonator coupled line filter. For the filter, reducing the cover height was seen to narrow the passband response and raise the amplitude of the filter's rejection band response. The numerical results of this research give an excellent prediction of this effect, whereas discrepancies are apparent in the CAD model predictions.

[5]Multiple lines are needed for broad-band measurements.

Acknowledgment

The authors thank E. Watkins, J. Schellenberg, and M. Tutt for their contributions to this work.

References

[1] L. P. Dunleavy and P. B. Katehi, "A generalized method for analyzing shielded thin microstrip discontinuities," pp. 1758–1766, this issue.

[2] R. L. Eisenhart, "A better microstrip connector," in *1978 IEEE MTT-S Dig.*, pp. 318–320.

[3] L. P. Dunleavy, "Discontinuity characterization in shielded microstrip: A theoretical and experimental study," Ph.D. dissertation, University of Michigan, Ann Arbor, Apr. 1988.

[4] N. R. Franzen and R. A. Speciale, "A new procedure for system calibration and error removal in automated *S*-parameter measurements," in *Proc. 5th European Microwave Conf.*, 1975, pp. 69–73.

[5] B. Bianco *et al.*, "Launcher and microstrip characterization," *IEEE Trans. Instrum. Meas.*, vol. IM 25, pp. 320–323, Dec. 1976.

[6] G. Engen and C. Hoer, "Thru-reflect-line: An improved technique for calibrating the six-port automatic network analyzer," *IEEE Trans. Microwave Theory Tech.*, vol. MTT-27, pp. 987–993, Dec. 1979.

[7] L. Dunleavy and P. Katehi, "Repeatability issues for de-embedding microstrip discontinuity *S*-parameter measurements by the TSD technique," in *Automatic RF Techniques Group (ARFTG) Conf. Dig.*, June 1986.

[8] E. Yamashita and K. Atsuki, "Analysis of microstrip-like transmission lines by nonuniform discretization of integral equations," *IEEE Trans. Microwave Theory Tech.*, vol. MTT-24, pp. 195–200, 1976.

[9] J. Snook, "Substrates for hybrid microelectronic applications," *Microwave Syst. News*, pp. 26–31, Feb. 1988.

[10] R. H. Jansen, and N. H. L. Koster, "Accurate results on the end effect of single and coupled lines for use in microwave circuit design," *Arch. Elek. Übertragung.*, vol. 34, pp. 453–459, 1980.

[11] T. Itoh, "Analysis of microstrip resonators," *IEEE Trans. Microwave Theory Tech.*, vol. MTT-22, pp. 946–951, 1974.

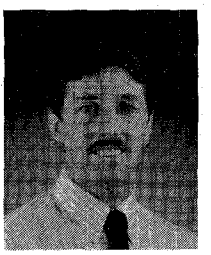

Lawrence P. Dunleavy was born in Detroit, MI, on September 16, 1959. He received the B.S.E.E. degree from Michigan Technological University, Houghton, in 1982 and the M.S.E.E. and Ph.D. degrees in electrical engineering from the University of Michigan, Ann Arbor, in 1984 and 1988, respectively. His Ph.D. research was in the area of numerical analysis and measurement of microstrip structures.

From 1982 to 1983 he worked at the ECI division of E-Systems Inc., St. Petersburg, FL,

where he provided production support and design engineering for hybrid microwave circuitry. In 1983 he began graduate studies at the University of Michigan under a Schlumberger Graduate Fellowship. In 1984 he joined Hughes Aircraft Company as part of the Howard Hughes Doctoral Fellowship program. At the Space and Communication Group of Hughes, El Segundo, CA, he worked on system analysis of a millimeter-wave phased array antenna. In 1985 he transferred to the Industrial Electronics Group of Hughes, Torrance, CA, where his current responsibilities include research and development of new techniques for microwave and millimeter-wave measurements, and the design of GaAs-based hybrid and monolithic circuits operating in the 10–40 GHz frequency range.

Dr. Dunleavy is a member of the IEEE MTT and AP-S societies, Tau Beta Pi, Sigma Xi, Eta Kappa Nu, and the Automatic RF Techniques Group (ARFTG).

Pisti B. Katehi (S'81–M'84) received the B.S.E.E. degree from the National Technical University of Athens, Greece, in 1977 and the M.S.E.E. and Ph.D. degrees from the University of California, Los Angeles, in 1981 and 1984 respectively.

In September 1984 she joined the faculty of the EECS Department of the University of Michigan, Ann Arbor, as an Assistant Professor. Since then, she has been involved in the modeling and computer-aided design of millimeter-wave, and near-millimeter-wave monolithic circuits and antennas.

In 1984 Dr. Katehi received the W. P. King Award and in 1985 the S. A. Schelkunoff Award from the Antennas and Propagation Society. In 1987 she received an NSF Presidential Young Investigator Award and a Young Scientist Fellowship awarded from URSI. Dr. Katehi is a member of IEEE AP-S, MTT-S and Sigma Xi.